J. Physiol. (Paris) 94 (2000) 375–390

PII: S0928-4257(00)01085-8/FLA

To beat or not to beat: A decision taken at the network level

Yair Manor[a], Yosef Yarom[b]*, Edith Chorev[b], Anna Devor[b]

[a]*Life Sciences Department and Zlotowski Center for Neuroscience, Ben-Gurion University of the Negev, Beer-Sheva 84105, Israel*
[b]*Dept of Neurobiology, Life Sciences Institute and the Center for Neuronal Computation, Hebrew University, Jerusalem 91904, Israel*

Received 9 July 2000; accepted 7 August 2000

Abstract – The cells of the inferior olivary nucleus, the sole source of the cerebellar climbing fibers, form a network of electrically coupled neurons. Experimental observations show that these neurons produce a large repertoire of electrical signals, among which sub-threshold oscillations of the membrane potential. Simultaneous recordings from pairs of neurons and optical imaging of voltage sensitive dyes show that sub-threshold activity occurs in synchrony throughout the network. The mechanism underlying the generation of the sub-threshold oscillations is not fully understood. Experimental observations suggest that the electrical coupling is essential but insufficient for their generation. Several theoretical mechanisms have been suggested to explain these observations. Up-to-date, the most realistic model is the heterogeneity model, that assumes a certain degree of heterogeneity among olivary neurons. The heterogeneity model proposes that sub-threshold oscillations are produced by electrical coupling of neurons with the same types of ionic conductances, but with different densities. The variability in channel densities yield neurons of different functional types. The main prediction of the model is that different functional types of neurons should be found in the inferior olive. Dynamic clamp experiments support this prediction. © 2000 Elsevier Science Ltd. Published by Éditions scientifiques et médicales Elsevier SAS

1. Introduction

Periodic activity is a feature shared by many neurons in the CNS. Oscillations are implicated in various functions, from information carriers to organizers of cell assemblies and internal clocks (see review in [8]). A key question is how these oscillations are produced. In general, oscillations can be either dictated by pacemaker elements or emerge from network activity (but these two possibilities are not mutually exclusive). The well documented rhythmic activity in the inferior olive (IO) is an example for a rhythm generated by an ensemble of neurons. When met with the experimental data, one is left with the impression that periodic activity in the inferior olive is a unique phenomenon. First, oscillations in the inferior olive are confined to this nucleus, being sub-threshold for firing. Second, the oscillations can be very regular, sometimes appearing as a remarkable sine wave. It is presumed that these oscillations serve as a time reference mechanism and process incoming information according to the on-going activity [11]. Third, it appears that the existence of the oscillations is crucially dependent on electrical connections between olivary neurons [10, 14], a prominent feature in this nucleus [12].

The electrophysiological properties of the inferior olivary neurons have been extensively studied over the last two decades [1, 2, 13–15, 25]. The picture that crystallizes from these studies is of a complex system endowed with the capability to generate a large repertoire of electrical activities. The cellular origin of the sub-threshold oscillation was tracked down to the low threshold calcium conductance, a characteristic feature of olivary neurons. This component, together with the electrical coupling, is essential to produce the sub-threshold oscillations. However, how these two ingredients are combined to yield the rhythmic activity is still not clear.

A decade ago, Yarom proposed that when damped oscillators are electrically coupled to each other, they might be capable of producing a sustained oscillation similar to the sub-threshold oscillations. An analog electrical circuit that captures the basic ideas of this verbal model showed that indeed sub-threshold oscillations can be generated by a network of coupled neurons [24], where each of the individual 'neurons' preserved stable state characteristics. Furthermore, by hybridizing the analog 'neurons' with a biological olivary neuron, it was demonstrated that the olivary neuron behaves as a genuine damped oscillator. However, one of the assumptions of this model was that the electrical coupling does not

* Correspondence and reprints.
E-mail address: Yarom@vms.huji.ac.il (Y. Yarom).

decrease the input resistance of the neurons, in contrast to the expected in neuronal systems. In principle, intrinsic currents could compensate for the reduced input resistance, but there is no real evidence to support such a mechanism.

Recently, several computational models were proposed to improve on the original ideas put forward by Yarom [17, 18, 21, 23]. Noteworthy is a theory proposed by Loewenstein et al. [17], where internal variables are potentially rhythmic, but the periodic behavior is expressed only when neurons are electrotonically coupled. Two models were constructed to demonstrate this theory. One of these models consists of two-compartment neurons. The 'somatic' compartment is endowed with active properties that allow it to produce oscillations. The 'dendritic' compartment is passive and acts to dampen the oscillations. When such neurons are electrically coupled through their dendritic compartments, sustained oscillations are produced. The second model consists of oscillation in intracellular calcium concentrations generated by a positive feedback loop between two calcium compartments. In this model the membrane voltage suppresses the oscillations. Electrical coupling between these neurons decreases the responsiveness of the membrane voltage, thereby unraveling the oscillatory change in intracellular calcium concentration. The latter is expressed as voltage oscillation via a mechanism of calcium dependent potassium conductance. The theory proposed by Loewenstein et al. is interesting because it explains how oscillations can be generated from electrical coupling of 'identical' quiescent neurons.

A more realistic model is based on the idea originally suggested in Manor et al. [18]. The basic assumption of this model is that although the olivary neurons contain the same ionic conductances, they differ in their channel densities. The model includes a single compartment, consisting of a leak and an instantaneous calcium conductance. The uniqueness of this model therefore lies in its simplicity, which facilitates an analytical analysis. The model proposes that heterogeneity in the constituent coupled elements is sufficient to generate oscillatory activity.

In this manuscript, we briefly review the electrophysiological properties of olivary neurons. We expand on the experimental observations that support a network origin of the sub-threshold oscillations. We then summarize the main findings of the heterogeneity model, and examine its predictions by using the dynamic clamp.

2. Methods

2.1. Electrophysiology

All experiments were done with the whole cell patch clamp method (or sharp electrodes where specified) in brain stem slices. Slice preparation was as described elsewhere [14]. To record sub-threshold oscillations we used mature (P14–P30) rats where rhythmic activity appeared with high probability. Electrophysiology on quiescent neurons was done on young (P8–P12) rats, where oscillation probability was low. Intracellular staining was done by intracellular injection of 0.5% neurobiotin, a low weight dye that crosses gap junctions.

2.2. Optical imaging

Slices were incubated for 20 min in a solution that contained the voltage sensitive styryl dye RH-414 (0.3 mM). A two-dimensional array of 128 photodiodes covered an area of 600×600 μm^2. The optical imaging system, data collection and analysis were described in details previously [5].

2.3. Modeling

The model was constructed from voltage clamp data extracted in brain slices of guinea pigs, as described previously [18]. Individual and pairs of neurons were simulated using xpp (software written by G.B. Ermentrout, see http://www.pitt.edu/~phase). For larger networks we used IONET, an object oriented software developed by one of us.

2.4. Dynamic clamp

The dynamic clamp technique [22] was used to introduce (or delete) model conductances into biological neurons. Briefly, a model conductance was formulated as a set of differential equations. Parameters for the model conductance were obtained from voltage clamp experiments. The artificial conductance (dependent both on voltage and time) was advanced in real time, using as input the on-going voltage of the cell. The corresponding current, calculated on-line as the product of the simulated conductance and the estimated driving force, was injected into the cell.

3. Cellular and network properties of the inferior olive

3.1. Electro-responsiveness of olivary neurons

The neurons in the IO nucleus are endowed with a variety of voltage-dependent ionic channels. These ionic properties produce sub- and supra-threshold activity not found in any other CNS neuron. In contrast to many other neurons in the CNS, the excitability of olivary neurons can increase by both depolarization and hyperpolarization. This is illustrated in *figure 1A*, where the intracellular response to a short pulse of current is shown for three different membrane potentials. At the resting membrane potential (− 62 mV; middle trace), a 10-ms, + 150 pA pulse generated a low threshold calcium spike, but no sodium spike was produced. When the membrane potential was displaced to a hyperpolarized level (bottom trace; − 72 mV), the same stimulus generated a low threshold calcium spike, which triggered a sodium action potential. A different response was obtained when the membrane potential was displaced to a depolarized level (top trace; − 47 mV). Here the stimulus produced a high threshold calcium spike, that was followed by a prolonged after hyperpolarization. This after hyperpolarization elicited a second calcium wave. If this secondary calcium wave was large enough, a sodium action potential was generated and a third after-wave was produced (top trace of *figure 1B*). A series of calcium waves (with damped amplitudes) could also be induced by preconditioning the olivary neuron with a negative current pulse (bottom three traces in *figure 1B*). The duration of this after-effect increased with the intensity of the preconditioning pulse. The neuron, thus, behaved as a damped oscillator.

Occasionally, the olivary neurons showed spontaneous, sub-threshold oscillations of membrane potential. The probability of oscillations depended on various factors, such as the saline composition

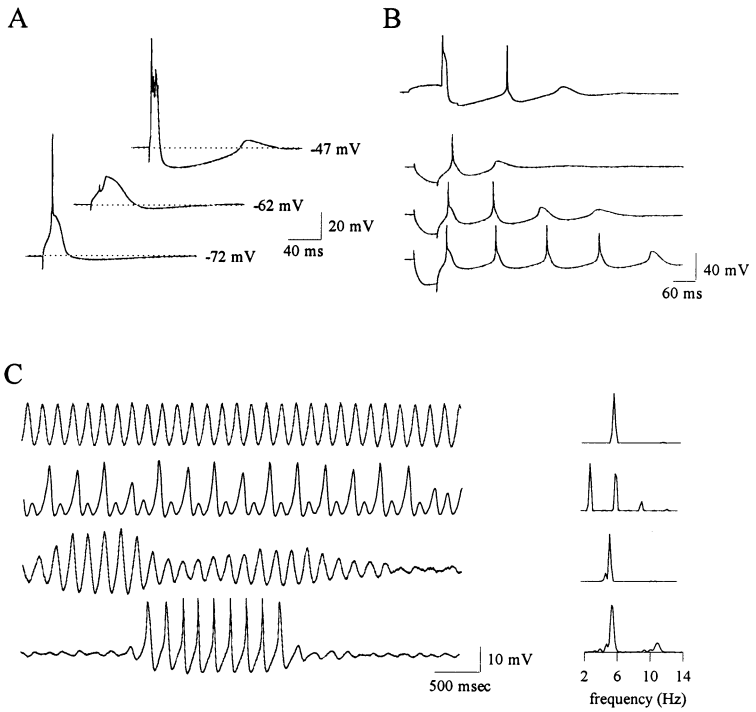

Figure 1. The electroresponsive properties of olivary neurons. **A**, Low and high threshold spikes dominate the electrical activity of olivary neurons. Intracellular voltage responses to positive current pulse (10 ms, + 150 pA) delivered at different holding potentials (dashed lines) are displayed. At resting level (− 62 mV) the stimulus failed to generate action potentials. At − 72 mV, the same stimulus induced a low threshold calcium spike. At − 47 mV, the stimulus triggered a high threshold calcium spike. **B**, Either depolarizing or hyperpolarizing pulses can generate damped oscillatory activity. Top trace shows rhythmic activity generated by depolarizing pulse. Bottom three traces show rhythmic activity generated by hyperpolarizing pulses. Note that in the bottom traces the duration of the oscillatory activity increased with the intensity of the hyperpolarizing pulse. **C**, The spontaneous sub-threshold oscillations in olivary neurons appear in different frequency, shape and amplitude. Traces were recorded from different neurons in different slices. Corresponding power spectra are shown on the right.

or the age of the animals. These oscillations (later in this text referred as STOs) varied in frequency (between 1.5 and 8 Hz) and amplitude (from 0.5 to 25 mV). The STOs showed different patterns: almost sinusoidal (*figure 3C*, top trace), period doubling (*figure 3C*, 2nd trace), beating (*figure 3C*, 3rd trace) or intermittent oscillations (*figure 3C*, bottom trace). In this last case, the activity consisted of epochs of oscillations separated by silent periods, lasting from seconds to minutes.

Neurons recorded from the same slices tended to display STO with similar shape, amplitude and frequency. However, STOs recorded in different slices, albeit the same animal, sometimes differed dramatically. It is possible that the variability in oscillation pattern reflects a reorganization of the electrical activity that follows from the disruption of the fine structure of the electrical coupling.

3.2. Electrotonic coupling in the IO nucleus

To demonstrate the electrical coupling of neurons in the IO nucleus, we recorded from pairs of somata in mature animals. In 40% of the pairs, electrical coupling was observed (*figure 2*). In A, hyperpolarizing pulses were injected into one of the two neurons (left: cell '1'; right: cell '2') and the response was recorded in both cells. The response in the non-stimulated cell (left: cell '2'; right: cell '1') was smaller and slower, as expected from a direct and non-rectifying electrical coupling between the two cells. In average, the coupling coefficient, defined as the ratio of steady-state voltage responses, was 0.03 (minimum: 0.01; maximum: 0.11; $n = 21$). Usually the coupling was symmetrical but, as expected, the coupling coefficient depended on the input resistance of the post-junctional cell. Because the input resistance of olivary neurons depends on the membrane potential, an 'apparent' voltage dependence of the coupling coefficient was observed.

Electrical coupling could also be demonstrated when a high threshold calcium spike was evoked in one of the two cells. The response in the post-junctional cell had a characteristic biphasic waveform that reflected the low-pass filtering of the voltage response elicited in the stimulated cell: the positive and negative phases correspond to the high threshold calcium spike and the prolonged after-hyperpolarization, respectively (*figure 2B*).

Figure 2C shows an interesting case where the two cells displayed spontaneous and synchronous biphasic responses, resembling the post-junctional waveforms shown in *figure 2B*. We did not observe direct coupling between these two neurons (data not shown). Nevertheless, the two responses were similar in shape and comparable in amplitude – as if generated by a common source. We therefore conjecture that the two neurons were electrically coupled to a third neuron, which produced a spontaneous high threshold spike.

Figure 2B and *C* illustrates an important point: a single compound action potential either evoked or spontaneously generated in a neuron is insufficient to elicit an action potential in a post-junctional neuron. This is not surprising, due to the low coupling coefficient. However, this weak coupling is raising questions regarding the functional role of this interaction (see Discussion).

The extent of electrical coupling between olivary neurons could be estimated by injecting olivary neurons with low weight dyes that cross gap junctions, such as neurobiotin. In *figure 2D*, one cell was injected with neurobiotin. Two other neurons (marked by arrows) were indirectly stained, suggesting that the labeled cell is electrically coupled to at least two neurons. We note that, as in other preparations [4], exposure to high-pH medium increased the extent of dye coupling and hence the number of indirectly labeled cells.

3.3. Sub-threshold oscillations emerge from a network of electrically coupled olivary neurons

A fundamental question of olivary function is the source of the STOs. We propose that oscillations emerge from network activity, based on the following lines of evidence.

In cases where oscillations are spontaneous, treatments that affected the single cell did not disrupt the rhythmic activity. *Figure 3A* shows an example where an oscillating cell was injected with DC negative currents that displaced the membrane potential to different hyperpolarized levels. Although the amplitude of the oscillations increased with hyperpolarization, the frequency was not changed. Moreover, current perturbation in an oscillating neuron did not interfere with the oscillations. This is demonstrated in *figure 3B* where two pairs of superimposed traces are shown. In one trace, the neuron showed unperturbed STOs. In the second trace, the neuron was injected with a stimulus that produced a high threshold calcium spike. It can be seen that independent of the stimulation time, these perturbations did not affect the phase or frequency of the STOs.

In contrast, global treatments that affected the whole population did disrupt the STOs. As an

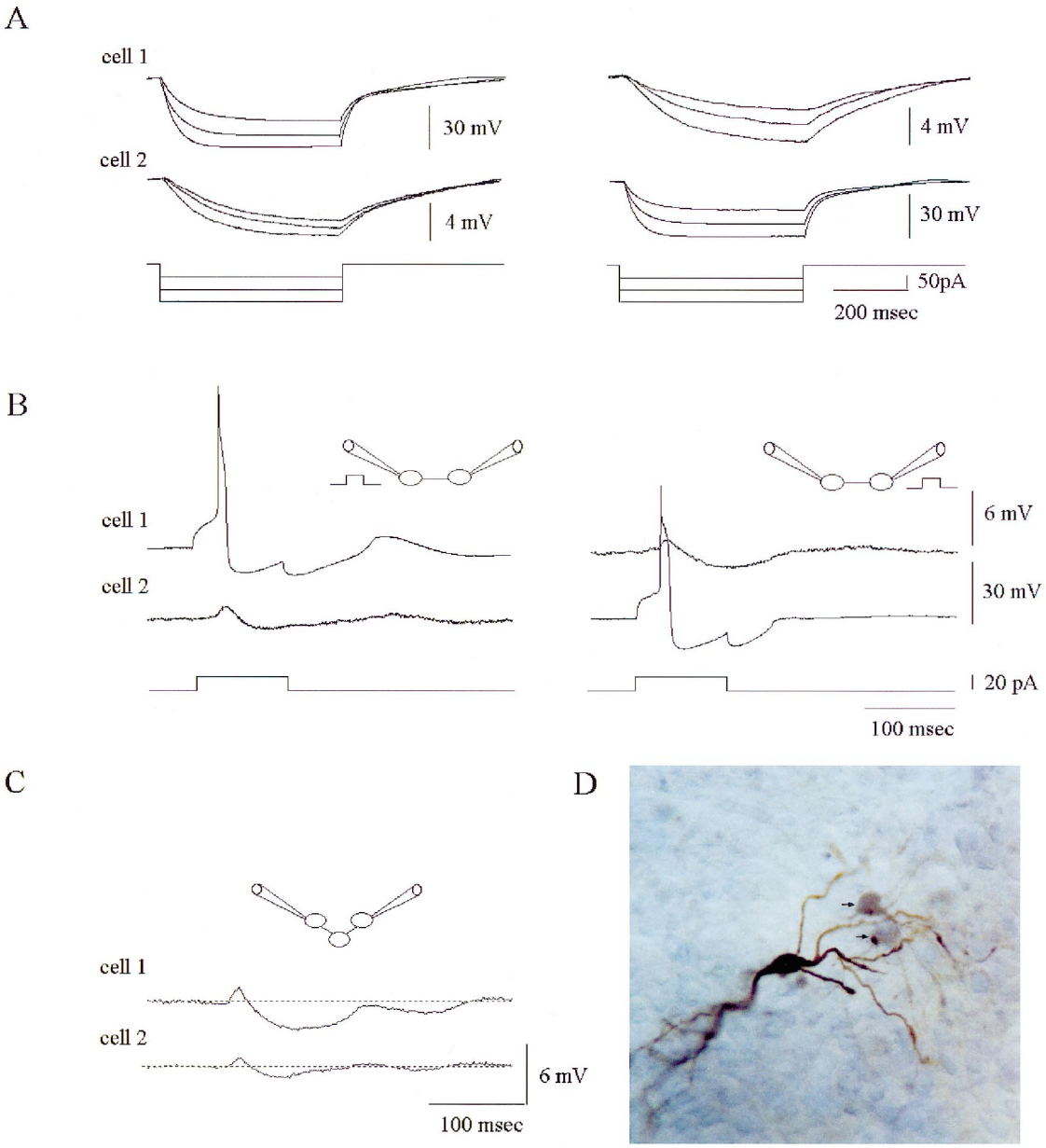

Figure 2. Inferior olivary neurons are electrically coupled. **A**, Prolonged current injections demonstrate direct current flow between two neurons that were simultaneously recorded. Negative current pulses of various intensities were injected into cell '1' (left column) or cell '2' (right column). Note that the voltage response in the post-junctional cell has a lower amplitude and slower time course. **B**, Action potentials are poorly transmitted via the electrical synapse. Action potentials were elicited by depolarizing current pulses (bottom traces) in either of the two cells (left and right columns). The insets indicate which one of the cells was stimulated directly. Note that as expected from electrical synapses the transmission of the prolonged after hyperpolarization phase is much better than the brief depolarizing phase of the action potential. **C**, Simultaneous recording from two olivary neurons revealed spontaneous, sub-threshold events that occurred synchronously in both cells. The shape and amplitude of these events resembled the post-junctional cell response to a spike in the pre-junctional cell (see **B**). The inset shows a schematic network arrangement that could account for these events. **D**, A single inferior olivary neuron was injected intracellularly with neurobiotin. Two other cells (arrows) were labeled indirectly by dye passing through gap junctions.

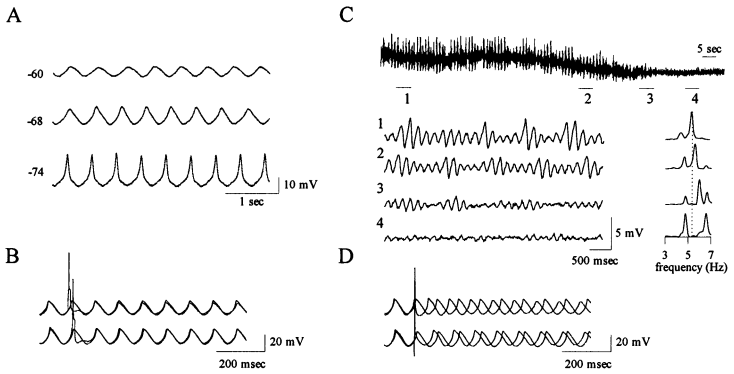

Figure 3. The oscillatory activity is modulated by a treatment that affects a large population of neurons. **A**, The sub-threshold oscillations are unaffected by the membrane potential. The sub-threshold oscillations of an olivary neuron were recorded while the membrane potential was shifted to different levels (as indicated to the left of the traces) by DC current injection. Note that the waveform changed but the frequency was not affected. **B**, Action potentials generated by current injection to a single cell do not affect the oscillations. Each panel superimposes two traces with and without current injection. The two traces were aligned by the peak of the first (left) wave. Action potentials were generated at the peak of the wave (bottom traces) or the upstroke of the wave (top traces). **C**, Lowering the extracellular K^+ concentration, a procedure that hyperpolarizes a large population of neurons, abolishes the sub-threshold oscillations. A continuous 2-min recording of intracellular voltage is shown at top. The time fragments indicated by bars and denoted as 1,2,3,4 are shown below at faster recording sweep. Corresponding normalized power spectra are shown on the right. **D**, Action potentials generated by extracellular stimulation induce a phase shift in the sub-threshold oscillations. Presentation is as in **B**. Note that the extent of the phase shift depends on the time of stimulation.

example, we show how global hyperpolarization abolishes the rhythmic activity (*figure 3C*). The top trace shows a slow sweep of intracellular activity following substitution of the saline with low potassium saline. As a result, the voltage of the cell gradually declined, and the oscillations were abolished (compare time sections '1' and '4'). To gain insight into how rhythmic activity was lost, we expand the time bases of sections '1', '2', '3' and '4', and plot the associated normalized power spectra. It can be seen that the amplitude of oscillations decayed, the pattern of oscillations changed and the main frequency component moderately shifted to the right.

Extracellular stimulation of the slice is another treatment that affects the whole population of cells (*figure 3D*). This global stimulation advanced the phase of the STOs (compare superimposed traces of perturbed and unperturbed STOs recorded in the same neuron). The extent of the shift depended on the stimulus timing, relative to the STO phase (compare top and bottom traces).

Another support for the network source of STOs comes from the synchrony level between oscillations recorded simultaneously from pairs of neurons. *Figure 4* shows an example of an intermittent oscillation recorded in a pair of adjacent neurons (distance between somata: 15 μm). In this case, the epochs of oscillations lasted tens of seconds, during which prominent amplitude modulation was observed in synchrony in both cells (top traces). Examination of time segments presented at a faster sweep (bottom traces) reveals the perfect synchronicity of the STOs. Such a behavior can be expected only if oscillations are the result of network activity (see Discussion).

To examine the synchronicity across larger populations of olivary cells, we used optical imaging of slices stained with voltage sensitive dyes (see Methods). An example is shown in *figure 5A*, where spontaneous synchronous activity was observed over an area of 200×400 μm. Global

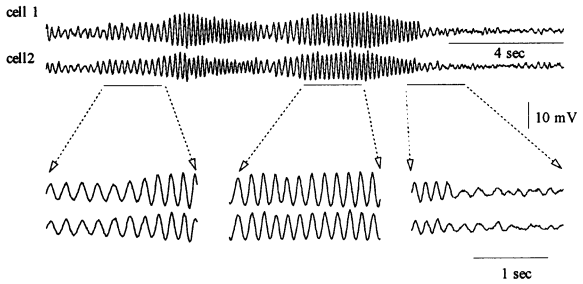

Figure 4. In phase appearance of sub-threshold oscillations. Simultaneous recordings from two intermittently oscillating neurons. The epoch of oscillation lasted for several seconds with a prominent amplitude modulation that occurred simultaneously in both cells. An extended time display of the time segments marked by bars shows that the sub-threshold oscillations occurred in phase in both cells.

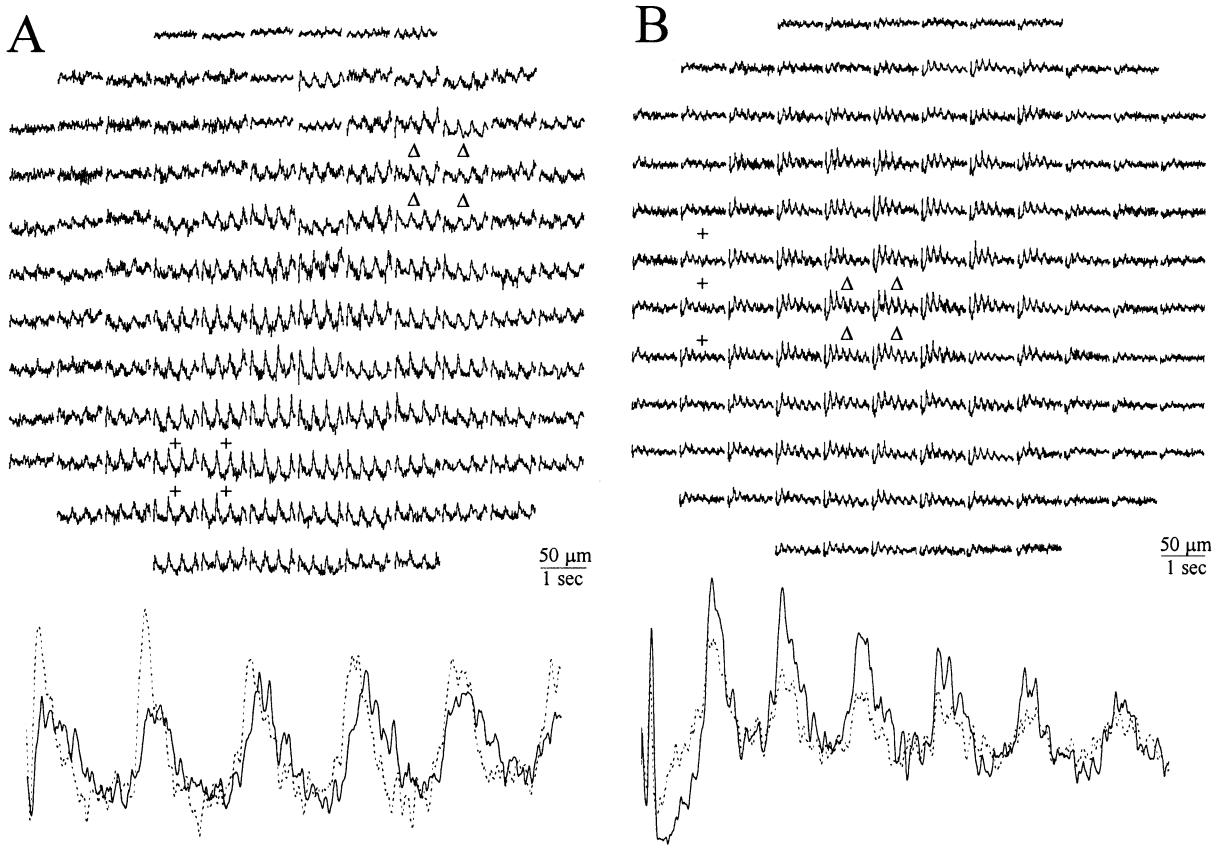

Figure 5. Optical imaging of the sub-threshold oscillations. The absolute change in fluorescence is measured by a photodiode array, in a brain stem slice stained with RH-414. Each trace represents the change in fluorescence recorded by a single photodiode as a function of time in its relative location (an area of 50×50 μm). **A**, Spontaneous oscillations. One second of continuous recordings shows 6-Hz oscillations. The averages of four diodes marked by triangles and crosses are shown in faster sweep as solid and dashed lines, respectively (lower traces). Note that the oscillations are almost in phase. **B**, Evoked oscillations. The response of olivary neurons to a single extracellular stimulus delivered by a bipolar electrode (located to the left of the recording area) was averaged ($n = 3$). Display is as in **A**. Note that the direct response to the stimulus (first spike-like response) has different characteristics than the following damped oscillatory waves.

rhythmic activity as seen in *figure 5A* was observed in only 10% of the slices. Moreover, in these slices the activity was not always observed, but followed an intermittent pattern. This result seems surprising, since intracellular recordings revealed a much larger proportion of the olivary neurons that showed STOs (50% in mature animals). A plausible explanation for this discrepancy is that in our system, each diode integrates voltage signals scattered across 50×50 μm. Hence, only in-phase oscillations are detected by the imaging system. This explanation is supported by the experiment shown in *figure 5B*. Here the oscillatory activity was evoked by extracellular stimulation, which entrains neurons to in-phase oscillations, as was demonstrated in *figure 3D*. Note that the oscillatory activity was damped, implying that the in-phase synchronization was only temporary. The lower traces in A and B show pairs of superimposed traces recorded from Δ and + . It illustrates that two remote areas were synchronized during the recording period.

Experimental data reviewed above demonstrate that the STOs are a population phenomenon, which are critically dependent on electrical connections between the olivary neurons.

4. The sub-threshold oscillations: a computational approach

In our experimental work, we have identified the major ingredients participating in the formation of synchronized, in-phase STOs. However, how these

ingredients combine to produce a coherent behavior is still not fully understood. To gain insights on the mechanism underlying the generation of STOs, we developed a computational model that explains how low amplitude oscillations emerge from electrical coupling of otherwise quiescent neurons [18]. Below we review this model, extend it to a population of neurons and use the dynamic clamp approach to examine its predictions.

4.1. Biological variability in the electrical properties of olivary neurons

The model was inspired by the observation that some of the olivary properties are highly variable. For example, in recordings with sharp microelectrodes we measured input resistance ranging from 10 to 70 M, and membrane time constant ranging from 2 to 10 ms (*figure 6A*). An important question is whether this variability is due to variations in the intrinsic properties of the cells, or to different number of electrically coupled neurons. Indirect evidence for the source of this variability can be drawn from measurements of cellular properties that are totally dependent on channel densities, and hence not affected by network structure. One such property is the resonance frequency, which is the frequency at which an input signal yields a maximal response. Recently it has been proposed that, in neurons exhibiting resonance, the resonance is determined by the membrane time constant and the time constant of a resonant conductance [9]. If intrinsic (passive or active) properties of olivary neurons were identical, we would not expect variability in resonance frequencies. However, olivary neurons are highly variable in their resonance properties, the resonant frequency ranging from 2 to 10 Hz [10]. According to Hutcheon and Yarom [9], the variability in resonance frequencies could be explained by variability in leak conductance (affecting the membrane time constant) or variability in the time dependent properties of the low threshold calcium conductance (namely, the time constant of inactivation).

4.2. The single cell model

The single cell model consisted of two ionic conductances, a leak conductance and an inacti-

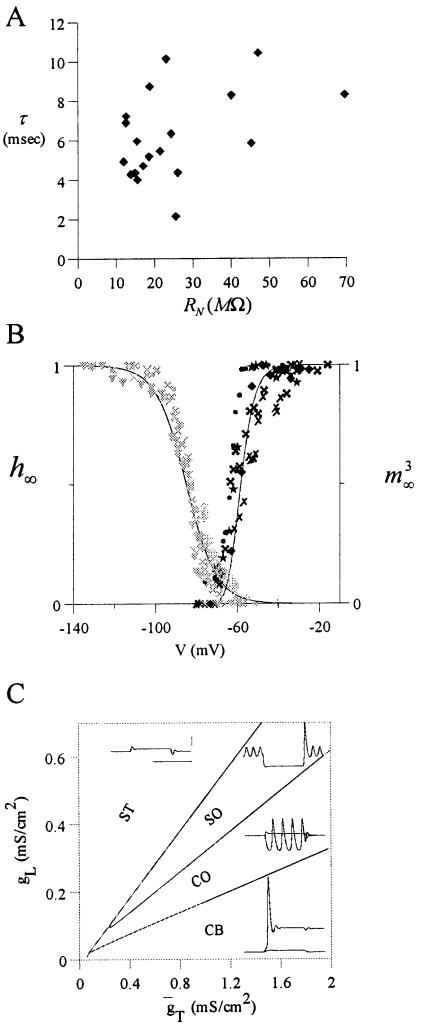

Figure 6. Construction of an experimentally-based model of the single neuron. **A**, Membrane time constant (τ_M) and input resistance (R_N) of olivary neurons were measured in current clamp with sharp microelectrodes. **B**, Activation and inactivation curves were extracted from voltage clamp experiments in several olivary neurons. Activation (gray symbols) and inactivation (black symbols) data were fit with Boltzman-like equations (m^3_∞ and h_∞, respectively). **C**, The single cell model consisted of two ionic conductances, a leak conductance and a low threshold calcium conductance. Different combinations of leak conductance (g_L) and maximal calcium conductance ($\bar{g}_T$) yielded four types of neurons, as shown on the $g_L - \bar{g}_T$ plane. Stable cells (ST) corresponded to neurons, which had a single stable fixed point, and could not be destabilized by current injection. Spontaneous oscillators (SO) oscillated with no current injection. Negative or positive current injection abolished the oscillations. Conditional oscillators (CO) were stable at resting potential, but produced oscillations when they were injected with negative current. Conditional bistable (CB) cells converged to one of two stable membrane potentials, depending on initial conditions. Insets show examples of each type of cells. Scale bars: 0.5 s, 5 mV.

vating calcium conductance. The following set of differential equations was used:

$$-C\,\mathrm{d}V/\mathrm{d}t = g_{\mathrm{L}}(V-E_{\mathrm{L}}) + \bar{g}_{\mathrm{T}}m^3(V)h \times (V-E_{\mathrm{Ca}}) - I_{\mathrm{ext}} \quad (1)$$

$$\mathrm{d}h/\mathrm{d}t = (h_{\infty}(V)-h)/\tau_h(V) \quad (2)$$

where C is the specific membrane capacitance, V the membrane potential, g_{L} and $\bar{g}_{\mathrm{T}}$ the leak and maximal calcium conductances, $E_{\mathrm{L}}$and E_{Ca} the leak and calcium batteries, and m and h the activation and inactivation variables of the calcium conductance (for a detailed description of the single cell model see [18]).

Activation-inactivation curves (m_{∞}, h_{∞}) and the voltage dependence of the inactivation time constant (τ_h) were extracted from data obtained in voltage clamp experiments (*figure 6B*). We examined the behavior of the single cell model as function of the leak and maximal low threshold calcium conductances (g_{L} and $\bar{g}_{\mathrm{T}}$, respectively). Different combinations of g_{L} and $\bar{g}_{\mathrm{T}}$ yielded four distinct behaviors of the single cell, categorized with respect to their response to current injection. In *figure 6C*, we identified four continuous regions in the $g_{\mathrm{L}}-\bar{g}_{\mathrm{T}}$ space, each region corresponding to a different type of cell (see insets). We labeled these regions as ST (stable cells), SO (spontaneous oscillators), CO (conditional oscillators) and CB (conditional bistable cells). It should be noted that the particular segmentation shown in *figure 6C* depends on the parameters of the model, which were mostly extracted from the experiments.

4.3. Oscillations emerge from the electrical coupling of neurons from different types

We first examined the simple case of two electrically coupled cells. To introduce the effect of electrical coupling of cell '2' onto cell '1', we modify equation (1) as follows:

$$-C\,\mathrm{d}V_1/\mathrm{d}t = g_{\mathrm{L}}(V_1-E_{\mathrm{L}}) + \bar{g}_{\mathrm{T}}m^3(V_1)h(V_1-E_{\mathrm{Ca}}) + g_{\mathrm{coup}}(V_1-V_2) - I_{\mathrm{ext}}$$

where V_1 and V_2 are the membrane potentials of the two cells and g_{coup} the coupling conductance. A similar equation is used to describe the voltage of cell '2'.

We formulated a rule of thumb, which we used to predict which pairs can produce oscillations, and which pairs fail to do so. The rule states that oscillations can be produced if two conditions are satisfied: (1) the line that connects the two cells in the $g_{\mathrm{L}}-\bar{g}_{\mathrm{T}}$ plane crosses the SO region; (2) the center of this line (corresponding to an 'average' cell) falls in the SO or ST regions. If the average falls in the SO region, oscillations are generated when the coupling conductance is larger than some threshold value. For example, in *figure 7A*, one of the cells is a stable cell (triangle), the other cell is a conditional oscillator (circle). The average cell ('x') lies in the SO region. When the coupling is larger than 0.1, the pair produces oscillation (3rd and 4th pair of traces). If, on the other hand, the average cell is a stable cell (residing in ST, *figure 7B*), oscillations are generated when the coupling conductance is restricted to a finite range of values. In agreement with the rule of thumb, the pair is quiescent when the coupling is small (top pair of traces) or strong (bottom pair of traces). In an intermediate range, the two cells generate a sustained oscillation.

The above analysis demonstrates the ability of electrical coupling to generate oscillation between two neurons. Because gap junctions are abundant in the inferior olive nucleus, olivary neurons are probably extensively coupled. Hence, we now extend this analysis to larger networks.

When the number of coupled cells is larger than two, different connectivity patterns are possible (see section 4.5). The simplest case possible is when all neurons are coupled to all other neurons (a connectivity type known as 'all-to-all'). We randomly drew combinations of g_{L} and $\bar{g}_{\mathrm{T}}$ values, assigned these values to model neurons, connected these neurons in the all-to-all configuration and modeled the network activity (*figure 7C*). Traces in this figure show, for different coupling strengths, the time courses of membrane potentials in two representative neurons of the cluster, a spontaneous oscillator (circle) and a conditional oscillator (triangle). As the all-to-all coupling was slightly increased above 0, the two cells produced rhythmic activity in a 'beating' (or amplitude modulated) pattern (2nd pair of traces from top). Interestingly, when the all-to-all coupling was further increased, the two cells stop their oscillatory behavior (3rd pair of traces from top). With strong all-to-all coupling, the two cells resume their oscillations – as expected from the properties of the population average ('x').

The results presented in *figure 7C* show that a population of several electrically all-to-all coupled neurons differed from a pair of coupled neurons, in that: (1) complex oscillatory patterns could be produced; and (2) oscillations could appear in several distinct ranges of electrical coupling values. We note that complex patterns of oscillation, such as shown in *figure 7C* (2nd pair of traces from

top), are occasionally seen in olivary slices (see for example *figures 1C* and *11A*).

4.4. The dependence of network oscillation on number of neurons

As stated previously, STOs are observed only occasionally. We hypothesize that the appearance of STOs depends on the size of the intact network, in individual slices. We therefore studied the capability of an olivary network to produce oscillations, as function of network size (i.e. the number of neurons, n).

Towards this end, we computed the probability of all-to-all networks of different size to produce oscillations. *Figure 8* shows the oscillation probability (P) as function of network size (n). The probability of a single neuron ($n = 1$) to produce oscillations was 0.26. This number is expected from the intersection of the SO region with the two-dimensional Gaussian distribution chosen for these simulations (*figure 8B*). As the size of the network increased, at first the probability 'decreased' to a minimal value of 0.01 at $n = 10$. This effect is explained by the increase of load when the number of cells is increased. Further increase in network size reversed this trend, and the probability 'increased' to a value of 0.87 at $n = 100$. It is

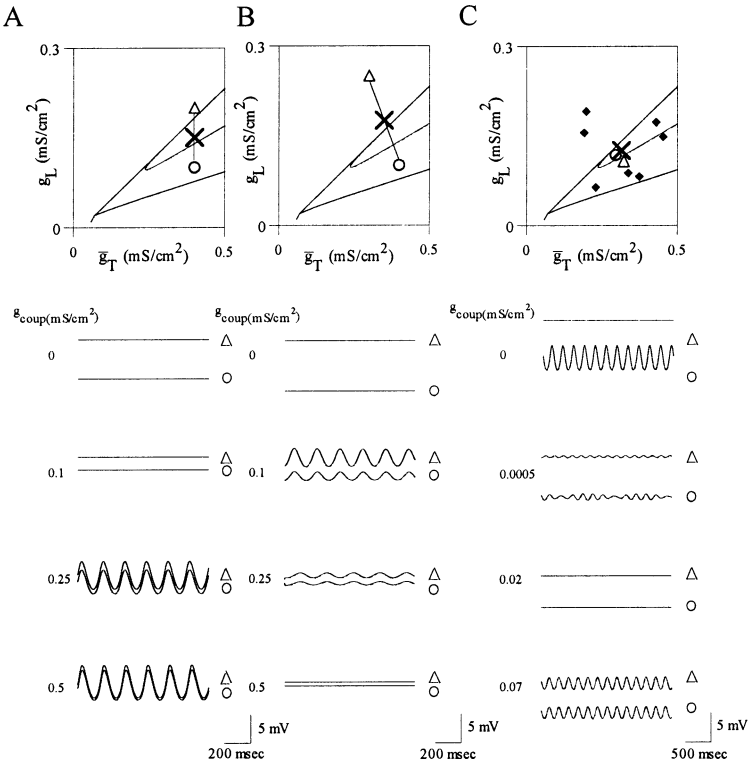

Figure 7. Low amplitude oscillations emerge from electrical coupling of neurons with different channel densities. Columns represent different model networks of neurons. Insets at the top of each column show the cells' conductances, superimposed on the $g_L - \bar{g}_T$ plane. 'X' represents the average conductances. Rows show the voltage time courses of representative cells when different coupling conductances (g_{coup}) are used. **A**, The network consisted of two electrically coupled cells: a stable cell (triangle) and a conditional oscillator (circle). When g_{coup} was 0 (no coupling) or 0.1 mS · cm^{-2}, the two cells were quiescent (top two pairs of traces). Oscillations were produced when g_{coup} was equal to 0.25 and 0.5 mS · cm^{-2} (bottom two pairs of traces). The average conductances ('X') fall in the spontaneous oscillator zone. **B**, Same as in **A**, but the average conductances fall in the stable zone. In this case, oscillations were produced when g_{coup} was equal to 0.1 and 0.25 mS · cm^{-2} (middle two pairs of traces), but not when g_{coup} was 0 (top pair of traces) or 0.5 mS · cm^{-2} (bottom pair of traces). **C**, The network consisted of nine cells coupled in an all-to-all connectivity (◆, $n = 7$; △ and ○ in inset). △ and ○ are a conditional oscillator and an oscillator, respectively. A pair of traces shows the voltage time courses of △ and ○ with different coupling values. Note that the coupling values are different than in **A** and **B**. When g_{coup} was zero, w as quiescent △ and ○ was oscillating. When $g_{coup} = 0.0005$ mS · cm^{-2}, the two cells showed a beating pattern. When $g_{coup} = 0.02$ mS · cm^{-2}, both cells were quiescent. Both cells produced oscillations when $g_{coup} = 0.07$ mS · cm^{-2}. Note that the population average ('X') is in the spontaneous oscillator zone.

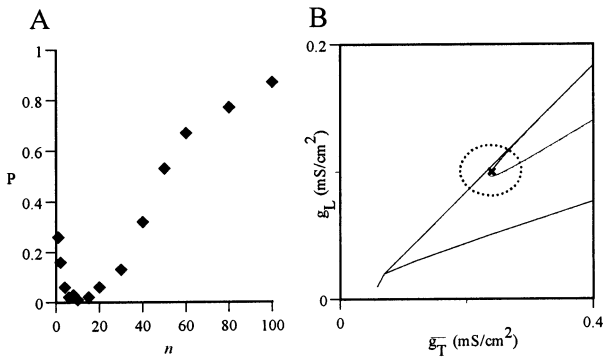

Figure 8. A, Oscillation probability of an all-to-all network depends on the network size. For a model network of size n, we randomly drew n combinations of $\bar{g}_T$ and g_L values from the two-dimensional Gaussian distribution $\bar{g}_T = 0.24 \pm 0.05$ ($\mu \pm \sigma$); $g_L = 0.1 \pm 0.02$ ($\mu \pm \sigma$) and assigned each conductance combination to a different model neuron. **B**, The population average (X) and the population variability (1σ, dotted circle) are superimposed on the $g_L - \bar{g}_T$ plane. We coupled n neurons in an all-to-all connectivity, with a moderate coupling strength of 0.04 mS · cm^{-2}. We then ran 100 simulations, each with a different collection of randomly selected $g_L - \bar{g}_T$ combinations, and calculated the probability (P) of a network of size n to produce sustained oscillations. When $n = 1$, P was 0.26. It decreased to 0.01 as n increased to 10, and then increased towards 1 as n was further increased.

likely that the increase in oscillation probability is due to the formation of oscillatory clusters (neurons, or groups of neurons, that form oscillations not because they are spontaneous oscillators, but because of their pairing – such as described in *figure 7A* and *B*).

4.5. What is the connectivity pattern within the olivary nucleus?

The connectivity pattern within the inferior olive is unknown. But does this anatomical organization matters at all to the network function? A related question is: can one infer the connectivity from the response of the network to experimental manipulation?

In *figure 9*, we show the response of a model neuron to negative current injection when it was embedded in a 64-neurons network that produced rhythmic activity. In *figure 9A* the 64 neurons were coupled in an all-to-all connectivity, whereas in *figure 9B* the connectivity was of the next-nearest-neighbor type: the network was organized in a two-dimensional matrix; each cell was coupled only to its immediate neighbors. In the all-to-all case, all neurons oscillated with the same frequency and phase. In contrast, in the next-nearest-neighbor case, neurons oscillated at the same frequency but small phase shifts could be observed (data not shown). Another qualitative difference between the two networks can be seen in the responses of the neuron to current injection. In the case of an all-to-all connectivity, larger current injection resulted in larger oscillations of smaller frequencies. When the current injection exceeded some value, the oscillations were abolished (the frequency decreased to 0). In contrast, in the next-nearest-neighbor connectivity the amplitude of the oscillations first increased, and then decreased. The frequency of oscillations was not affected.

These last results were more similar to the experimental behavior. First, as in the experiments (*figure 3A*) the STOs could not be abolished by current injection in a single neuron. Second, when large current values were injected the oscillations diminished, but through a decaying effect on the amplitude and not on the frequency. This result resembles the behavior of the biological system, when it is subject to a global treatment that lowers the membrane potential of all olivary neurons (*figure 3C*).

In summary, our simulation results suggest that the connectivity structure affects both the activity pattern and the response of the network to current perturbation.

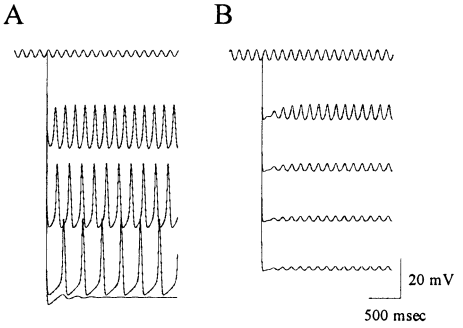

Figure 9. Voltage response of different model networks to current perturbation of a single cell. **A**, Voltage traces of a model cell in an all-to-all network of 64 coupled neurons (coupling conductance of each gap junction: 0.01 mS · cm^{-2}) is shown for stimulation currents of 0, −10, −20, −30, −32 μA · cm^{-2}. At current values larger than −32 μA · cm^{-2}, oscillations are abolished. **B**, Voltage traces of a model cell in a next-nearest-neighbor network of 64 coupled neurons (coupling conductance of each gap junction: 0.15 mS · cm^{-2}) is shown for stimulation currents of 0, −10, −20, −30, −40 μA · cm^{-2}.

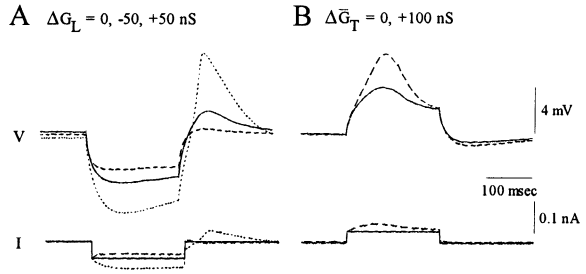

Figure 10. The dynamic clamp technique. **A**, A current pulse of -0.05 nA (I, bottom traces) is injected in an olivary cell in control (solid line), when a model leak conductance is artificially removed (dotted line, $\Delta g_L = -50$ nS) or added (dashed line, $\Delta g_L = +50$ nS). Top traces (V) show the voltage responses. **B**, A current pulse of $+0.03$ nA (I, bottom traces) is injected in control (solid line) and when a model low threshold calcium conductance is added (dashed line, $\Delta \bar{g}_T = +100$ nS).

4.6. Experimental validation of computational models with dynamic clamp

One of the predictions of the heterogeneity model is that the single cell can show four different types of behaviors, depending on the combination of its channel densities. To examine this prediction, our experimental approach was to 'transform' a biological cell from one type to another, by manipulating the combination of its ionic conductances. To this end, we took advantage of the dynamic clamp technique, which allows one to artificially add (or delete) model conductances to biological neurons (see Methods).

The basic principle of the dynamic clamp is illustrated in *figure 10*. In *figure 10A*, we demonstrate the effect of adding or removing a leak conductance from an olivary neuron. The response (V) to a current pulse injection (I) is shown in three cases: in 0 (solid line), -50 nS (dotted line) and $+50$ nS (dashed line). As expected from the effective change in leak conductance, the passive voltage response changed in agreement with the change in input resistance and time constant. Note also that the active rebound response changed appropriately. In *figure 10B* the low threshold calcium conductance was artificially boosted by adding 100 nS of modeled calcium conductance (model parameters extracted from voltage clamp experiments, see Methods). This simple experiment demonstrates our ability to modify the ionic conductances of an olivary neuron.

Armed with this tool we examined the possibility to modify the behavioral state of an olivary neuron. Indeed, as shown in *figure 11*, decreasing the leak conductance by 90 nS generated a low amplitude (~ 5 mV) irregular oscillation from an originally quiescent neuron. A further decrease of

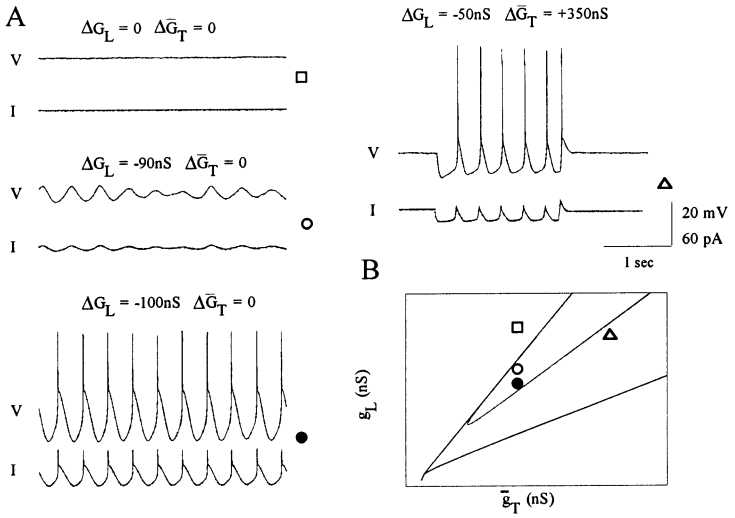

Figure 11. Incorporation of artificial conductances with the dynamic clamp 'transforms' an olivary neuron from one type to another. **A**, Voltage (top of each pair, V) and current (bottom of each pair, I) traces are shown for different incorporations of artificial conductances. In control ($\Delta \bar{g}_T = 0$, $\Delta g_L = 0$; open square), the neuron behaves as a stable cell. When leak conductance is reduced ($\Delta \bar{g}_T = 0$, $\Delta g_L = -90$ nS; open circle), the cell behaves as a spontaneous oscillator with only sub-threshold activity. When leak conductance is further reduced ($\Delta \bar{g}_T = 0$, $\Delta g_L = -100$ nS; closed circle), the cell shows spontaneous oscillations with supra-threshold activity. When leak conductance is less reduced but low threshold calcium conductance is increased ($\Delta \bar{g}_T = 350$ nS, $\Delta g_L = -50$ nS; triangle), the cell behaves as a conditional oscillator: it produces rhythmic activity upon injection of negative current. **B**, The transformations described in **A** are superimposed on a schematic drawing of the $g_L - \bar{g}_T$ plane.

the leak conductance by 10 nS enhanced (~ 30 mV) the oscillations, which triggered sodium spikes. Note also that the oscillations became regular. When the dynamic clamp was set to -50 nS leak conductance and $+350$ nS low threshold calcium conductance, a third category of behavior was revealed. Under this condition the cell exhibited oscillatory behavior only when the membrane potential was hyperpolarized. These changes in behavioral states corresponded to shifts from a stable state, to spontaneous oscillations, to a conditional oscillation – as predicted by the heterogeneity hypothesis and schematically illustrated in the $g_L - \bar{g}_T$ plane (*figure 11B*).

5. Discussion

Sub-threshold oscillations in the inferior olive are a remarkable phenomenon. Although experimentally studied for over two decades [10, 11, 13–15], the mechanism underlying these oscillations is still not clear. In this work we combined experimental and computational techniques to seek an answer for the following question: how are cellular and network properties integrated to generate this unique physiological behavior?

5.1. Electrical coupling in the inferior olive

One of the most striking observations in the inferior olive is the extensive electrical coupling between its neurons [7, 12]. In many other parts of the CNS, electrical coupling is associated with development [16, 19], and most electrical connections disappear when the animal maturates [6]. This general trend seems to work in reverse in the case of the inferior olive: gap junctions are mostly absent in embryonic stages, they form early and remain throughout the life-time of the animal [3]. It appears that electrical coupling in the inferior olive is functionally important for the normal, on-going life of the animal.

In dual recordings of olivary neurons, we found that olivary neurons can be directly coupled, or coupled through a third party. In any case, even in a direct coupling the coupling strength is quite weak. We demonstrated that it is too weak to allow an action potential in one neuron to elicit an action potential in another neuron. It is therefore not likely that the electrical coupling serves as an excitatory pathway such as occurs, for example, in the feeding circuit in *Aplysia* [20]. Another option is that electrical coupling synchronizes supra-threshold activity, but this possibility does not seem probable if one considers the low firing frequency of olivary neurons. What is, then, the functional role of electrical coupling?

5.2. A working hypothesis: electrical coupling is a mechanism of rhythmogenesis

Years of experimental work on olivary neurons have led us to realize that the individual olivary neuron, although equipped with a variety of nonlinear conductances, is not capable of producing sustained oscillations by itself. We therefore hypothesize that the oscillations are produced when olivary neurons are grouped via electrical coupling. Several lines of evidence support this hypothesis.

First, sub-threshold oscillations are not observed until P15–P20. Before this age, gap junctions in the inferior olive are scarce [3]. The developmental stage at which sub-threshold oscillations appear seems to correspond perfectly with the time of gap junction formation.

Second, in brain slices sub-threshold oscillations are observed in only 10 to 50% of the cases, depending on the age of the animal and the saline composition. We interpret this apparent variability as the result of the slicing procedure, which destroys the fine structure of the electrical coupling to various degrees. In addition to the occurrence of oscillations, the frequency and shape of the oscillations were also slice-specific. Our modeling work shows that, indeed, the network size determines the probability and pattern of the rhythmic activity.

Third, an action potential generated in a single neuron had no effect on the oscillations. In contrast, extracellular stimulation that elicited a synchronous volley of action potentials in a large number of neurons could reset the rhythm and shift the phase of the oscillations to various degrees, depending on the simulation time (relative to the oscillation phase). The phase was maximally shifted ($\sim 180°$) when the stimulus was given at the peak of the oscillation. The in-phase sub-threshold oscillations of olivary neurons, as found with optical imaging techniques, can explain this effect. At the peak of the oscillation many of the neurons are closest to their action potential thresholds. A stimulus given at this time drives a maximal number of neurons to fire action potentials, thereby inducing a large effect on the oscillations.

Fourth, hyperpolarization of a single neuron can modulate the amplitude of oscillations in this neuron, but it has no effect on the frequency or shape

of the oscillations. We recall that the low threshold calcium conductance, one of the major players in shaping the sub-threshold activity of olivary neurons, is voltage dependent. It may thus seem surprising, at first sight, that hyperpolarization of the single neuron has such a small effect on the sub-threshold oscillations. However, in a large ensemble the contribution of a single neuron to the network activity is expected to be small. A global hyperpolarization, on the other hand, affects the low threshold calcium conductance in all neurons of the network. Our network hypothesis predicts that, in this case, the sub-threshold rhythmic activity must be modified. Indeed, when the extracellular potassium concentration was decreased all olivary neurons in the slice were hyperpolarized. As a result, oscillations gradually diminished in amplitude, until rhythmic activity was completely lost. This effect is expected, because at hyperpolarized potentials the low threshold calcium conductance is not active.

Taken together, these experimental observations and their interpretation strongly support our working hypothesis that the olivary neurons are quiescent as individuals, and that electrical coupling of these neurons acts as a destabilizing factor to produce sub-threshold oscillatory activity.

5.3. Electrical coupling of heterogeneous neurons acts as a destabilizing factor

Gap-junctional coupling tends to reduce differences. In oscillating neurons, for example, strong electrical coupling synchronizes the oscillations and brings them to operate in phase. Because electrical coupling equalizes the membrane potential of neurons, it is widely accepted as a stabilizing agent. It is therefore not simple to see how electrical coupling of quiescent neurons could 'destabilize' their membrane potentials, as our working hypothesis implies.

To destabilize a stable system by electrical coupling, we intuitively understand that an additional feature must be considered. With an empirical approach, it is not easy to find this additional feature when it is not clear what to look for. This type of problem lends itself to modeling. Indeed, several theoretical studies have proposed solutions, as we briefly reviewed in the Introduction. In this manuscript we focused on one solution: the heterogeneity hypothesis. The heterogeneity model demonstrates that heterogeneity in the channel densities of neurons, endowed with the same types of conductances (as we believe is the case in the inferior olive), is sufficient to create oscillations when quiescent cells are electrically coupled. We emphasize that, in principle, relatively small differences in channel densities may suffice to produce the desired response.

5.4. The heterogeneity model reproduces experimental observations, and provides testable predictions

Our experimental data show that input resistances cover a wide range of values, and that membrane time constants are not correlated with these input resistances. This clearly indicates that a certain degree of heterogeneity does exist in the olivary nucleus, and that the basic assumption of the model is reasonable.

When expanded to a large network model, the heterogeneity model was able to duplicate many of the experimental observations. The response of the system to different perturbations was readily reproduced. For instance, the model demonstrated that oscillations cannot be abolished (or created) by current injection in a single neuron, but may be disrupted by a treatment that affects the whole population. The model illustrated that, as in the experimental data, oscillations could be almost sinusoidal, or follow more complex patterns such as beating and period doubling.

But the strength of this model is not merely in its competency to copy the olivary network. It is, perhaps more so, in its capacity to 'explain' the biological system. As an example we discuss the importance of the connectivity structure. The model clarified that the structure of the electrical coupling is an important factor. Where an all-to-all connectivity failed to reproduce the experimental behavior, a next-nearest-neighbor connectivity marked a success. On the other hand, the model demonstrated that the probability to find sub-threshold oscillations depends on the number of cells. All-to-all, better than next-nearest-neighbor, connectivity could explain the source of variability in the occurrence of oscillations in slices. It suggested that slices with less neurons would do poorly in showing oscillations, compared to slices with more neurons. We speculate that the neurons in the inferior olive are organized in a complicated connectivity pattern, perhaps a pattern that synthesizes the simplicity of the all-to-all connectivity with the more complex next-nearest-neighbor connectivity.

Most of all, the strength of the heterogeneity model lies in its ability to provide experimentally

testable predictions. The main prediction is that the electrical behavior of an individual olivary neuron depends on its channel density. With the aid of the dynamic clamp method, we modified the channel densities (added or deleted artificial leak or low threshold calcium conductances) of individual neurons. As predicted by the model, this manipulation enabled us to transform a neuron from a stable cell to a spontaneous or a conditional oscillator.

There is, however, one model prediction for which we could not find experimental support. The model predicts that at least some proportion of the olivary neurons should be spontaneous oscillators. We did not find such evidence. It is possible that spontaneous oscillators do exist among olivary neurons, but as predicted by the model they are unable to express their rhythmic behavior because of their coupling to stable neurons. An alternative possibility, though very speculative, is that during development natural selection is directed against rhythmic cells, leaving only stable cells or conditional oscillators.

6. Conclusions

We believe that we have a biologically plausible explanation to the mechanism of sub-threshold oscillations in the inferior olive. The heterogeneity model provides many predictions, which are experimentally testable. In the future we will concentrate our efforts to test these predictions.

In the field of neurosciences, theoreticians and experimentalists often find common ground. Some of them have even crossed the lines. This work is a successful example where an active dialog between experimentalists and theoreticians has led to the acquisition of insights profiting both sides. It illustrates that lines should not be crossed, but eliminated.

References

[1] Bal T., McCormick D.A., Synchronized oscillations in the inferior olive are controlled by the hyperpolarization-activated cation current I_h, J. Neurophysiol. 77 (1997) 3145–3156.

[2] Benardo L.S., Foster R.E., Oscillatory behavior in inferior olive neurons: mechanism, modulation, cell aggregates, Brain Res. Bull. 17 (1986) 773–784.

[3] Bleasel A.F., Pettigrew A.G., Development and properties of spontaneous oscillations of the membrane potential in inferior olivary neurons in the rat, Dev. Brain Res. (1991).

[4] Church J., Baimbridge K.G., Exposure to high-pH medium increases the incidence and extent of dye coupling between rat hippocampal CA1 pyramidal neurons *in vitro*, J. Neurosci. 11 (1991) 3289–3295.

[5] Cohen D., Yarom Y., Optical measurements of synchronized activity in mammalian isolated cerebellum, Neuroscience 94 (2000) 859–866.

[6] Connors B.W., Benardo L.S., Prince D.A., Coupling between neurons of the developing rat neocortex, J. Neurosci. 3 (1983) 773–782.

[7] De Zeeuw C.I., Ruigrok T.J.H., Holstege J.C., Jansen H.G., Voogd J., Intracellular labeling of neurons in the medial accessory olive of the cat: II. Ultrastructure of dendritic spines and their GABAergic innervation, J. Comp. Neurol. 300 (1990) 478–494.

[8] Gray C.M., Synchronous oscillations in neuronal systems: mechanisms and functions, J. Comp. Neurosci. 1 (1995) 11–38.

[9] Hutcheon B., Yarom Y., Resonance, oscillation and the intrinsic frequency preferences of neurons, Trends Neurosci. 23 (2000) 216–222.

[10] Lampl I., Yarom Y., Subthreshold oscillations and resonant behavior: two manifestations of the same mechanism, Neuroscience 78 (1997) 325–341.

[11] Lampl I., Yarom Y., Subthreshold oscillations of the membrane potential: a functional synchronizing and timing device, J. Neurophysiol. 70 (1993) 2181–2186.

[12] Llinas R., Baker R., Sotelo C., Electrotonic coupling between neurons in cat inferior olive, J. Neurophysiol. 37 (1974) 560–571.

[13] Llinas R., Yarom Y., Electrophysiology of mammalian inferior olivary neurones in vitro. Different types of voltage-dependent ionic conductances, J. Physiol. (Lond.) 315 (1981) 549–567.

[14] Llinas R., Yarom Y., Oscillatory properties of guinea-pig inferior olivary neurones and their pharmacological modulation: an in vitro study, J. Physiol. (Lond.) 376 (1986) 163–182.

[15] Llinas R., Yarom Y., Properties and distribution of ionic conductances generating electroresponsiveness of mammalian inferior olivary neurones in vitro, J. Physiol. (Lond.) 315 (1981) 569–584.

[16] Lo Turco J.J., Kriegstein A.R., Clusters of coupled neuroblasts in embryonic neocortex, Science 252 (1991) 563–566.

[17] Loewenstein J., Sompolinsky H., Yarom Y., A novel mechanism for the generation of sub-threshold oscillations in the inferior olive via symmetry breaking, Soc. Neurosci. Abstr. 368 (1999) 9.

[18] Manor Y., Rinzel J., Segev I., Yarom Y., Low-amplitude oscillations in the inferior olive: a model based on electrical coupling of neurons with heterogeneous channel densities, J. Neurophysiol. 77 (1997) 2736–2752.

[19] Peinado A., Yuste R., Katz L.C., Gap junctional communication and the development of local circuits in neocortex, Cereb. Cortex 3 (1993) 488–498.

[20] Perrins R., Weiss K.R., A cerebral central pattern generator in *Aplysia* and its connections with buccal feeding circuitry, J. Neurosci. 16 (1996) 7030–7045.

[21] Schweighofer N., Doya K., Kawato M., Electrophysiological properties of Inferior Olive neurons: a compartmental model, J. Neurophysiol. 82 (1999) 804–817.

[22] Sharp A.A., O'Neil M.B., Abbott L.F., Marder E., Dynamic clamp: computer-generated conductances in real neurons, J. Neurophysiol. 69 (1993) 992–995.

[23] Varona P., Torres J.J., Abarbanel H.D.J., Makarenko V.I., llinas R., Rabinovich M.I., Modeling collective oscillations in the inferior olive, Soc. Neurosci. Abstr. 368 (1999) 8.

[24] Yarom Y., Rhythmogenesis in a hybrid system-interconnecting an olivary neuron to an analog network of coupled oscillators, Neuroscience 44 (1991) 263–275.

[25] Yarom Y., Llinas R., Long-term modifiability of anomalous and delayed rectification in guinea pig inferior olivary neurons, J. Neurosci. 7 (1987) 1166–1177.